PNAS RESEARCH ARTICLE | ENGINEERING

Brittle and ductile yielding in soft materials

Krutarth M. Kamani[a,1] and Simon A. Rogers[a]

Edited by David Weitz, Harvard University, Cambridge, MA; received January 21, 2024; accepted April 29, 2024

Many soft materials yield under mechanical loading, but how this transition from solid-like behavior to liquid-like behavior occurs can vary significantly. Understanding the physics of yielding is of great interest for the behavior of biological, environmental, and industrial materials, including those used as inks in additive manufacturing and muds and soils. For some materials, the yielding transition is gradual, while others yield abruptly. We refer to these behaviors as being ductile and brittle. The key rheological signatures of brittle yielding include a stress overshoot in steady-shear-startup tests and a steep increase in the loss modulus during oscillatory amplitude sweeps. In this work, we show how this spectrum of yielding behaviors may be accounted for in a continuum model for yield stress materials by introducing a parameter we call the brittility factor. Physically, an increased brittility decreases the contribution of recoverable deformation to plastic deformation, which impacts the rate at which yielding occurs. The model predictions are successfully compared to results of different rheological protocols from a number of real yield stress fluids with different microstructures, indicating the general applicability of the phenomenon of brittility. Our study shows that the brittility of soft materials plays a critical role in determining the rate of the yielding transition and provides a simple tool for understanding its effects under various loading conditions.

brittle yielding | ductile yielding | soft materials | design criterion | yielding transition

Significance

Many soft materials yield under external loading or deformation, but not all yielding is the same. In this study, we account for ductile and brittle yielding by a single material parameter in a continuum constitutive model, indicating how a spectrum of yielding behaviors can be accounted for in soft materials. We show how this accounts for a range of behaviors observed for a variety of materials across a range of experimental protocols. The applicability of the model across materials indicates a potential universality in the ductile and brittle yielding rheology that is independent of microstructure. This finding has significant implications for material design for industrial, environmental, and biomedical applications.

Yielding is a process in which a soft material changes from being a viscoelastic solid, where deformations are recoverable, to deforming plastically, where deformations are unrecoverable under large applied loads. Such soft materials are known as yield stress fluids (YSFs). The ability to yield is common among systems as disparate as microgel suspensions, foams, emulsions, granular suspensions, and pastes (1–23). The ability of materials to yield and unyield is important for a wide variety of applications including direct ink writing (24–28), food and personal care products, filled rubbers, and many other industrial, biological, and environmental materials (29–33).

In the field of solid mechanics, extensive research has been conducted on the variations in failure mechanisms, distinguishing between ductile and brittle behaviors (34–36). Ductile failure is defined by the extent of plastic deformation sustained until fracture occurs. A material is categorized as being brittle if it undergoes minimal or no plastic deformation before fracturing. For soft materials, however, there is very little discussion on brittle and ductile yielding.

Despite their possible structural differences, YSFs show a remarkable similarity in their rheology. When deformed at a constant shear rate from rest, all YSFs display viscoelastic solid behavior at small stresses and strains and flow stably at large strains. However, the transition between those two states, the process of yielding, may be accompanied by an overshoot in the stress, the extent of which may be rate dependent and varies among materials (37–49). Overshoots in the stress observed during steady shear startup have been associated with brittle yielding (50–58).

Under application of constant stress, the viscosity of YSFs bifurcates about the yield stress (59–66). However, YSFs vary in their transient behavior through which the viscosity bifurcation is achieved. Some YSFs yield quickly under applied stress conditions, while others take considerable time before flow is established. This is typically referred to as "delayed yielding" (48, 60–62, 67–71) and is also associated with more brittle behavior (61, 72). In cases of delayed yielding, the application of stress leads to an initial decrease in the strain rate, indicating that the material may be tending toward cessation of flow. After some delay, there is a sudden and pronounced increase in the strain rate as the material yields.

When subjected to dynamic testing conditions achieved by oscillating the applied strain, the behavior of YSFs becomes more complex. Under conditions of small-amplitude oscillatory shear (SAOS), the dynamic moduli, which are proportional to the energy stored and dissipated, are approximately independent of the applied frequency for high volume fraction YSFs like glasses and jammed systems, while the response of lower

Author affiliations: [a]Department of Chemical and Biomolecular Engineering, University of Illinois at Urbana-Champaign, Champaign, IL 61801

Author contributions: K.M.K. and S.A.R. designed research; K.M.K. performed research; K.M.K. and S.A.R. analyzed data; and K.M.K. and S.A.R. wrote the paper.

The authors declare no competing interest.

This article is a PNAS Direct Submission.

[1]To whom correspondence may be addressed. Email: sarogers@illinois.edu.

This article contains supporting information online at https://www.pnas.org/lookup/suppl/doi:10.1073/pnas.2401409121/-/DCSupplemental.

Published May 22, 2024.

volume fraction solids like gels shows frequency-dependent behavior. As the applied strain amplitude is increased, an overshoot is observed in the loss modulus, which can gradually grow from small deformations, smoothly extending over a broad range of amplitudes, or initiate abruptly, rising steeply over only a very narrow range of amplitudes (23, 73–80). This phenomenon has been linked to the interaction potential of the local structure (23, 80). Across a range of materials, the overshoot in the loss modulus has been shown to be caused by a transition in how materials acquire strain, from predominantly recoverable at small strain amplitudes to predominantly unrecoverable at large strain amplitudes (79).

The response to oscillatory shearing from small to large amplitudes has been widely used to characterize behaviors of materials used as inks in direct ink writing, drilling fluids, and foods (81–86), among others. Ductile and brittle yielding in this experiment has been defined using the flow transition index (FTI), which is related to the steepness of the onset of the overshoot in the loss modulus. Steeper overshoots have smaller values of the FTI and have been noted as indicating brittle yielding. The applicability of the FTI is limited to average LAOS behavior represented by amplitude sweeps.

To understand the statistical physics behind the ductile and brittle yielding transition, theories have been put forth based on a critical point; a directed percolation transition (87); a spinodal (88–92); and a first-order transition in a replica theory (93, 94). These studies define ductile behavior as a smooth and gradual yielding transition, which is typically observed in less annealed samples (51). A brittle behavior is defined as one in which yielding occurs abruptly and catastrophically, as seen for well-annealed samples. Recently, it was reported that brittle yielding is accompanied by shear banding (51, 95, 96). Efforts to characterize and understand ductile and brittle yielding have been limited to protocols that apply either steady shear rates or steady stresses.

Phenomena associated with the rheology of brittle yielding, including stress overshoots in steady shear startup, delayed yielding in creep tests, and the steepness of the overshoot in the loss modulus under dynamic testing conditions, have primarily been studied in isolation. Even though they have all been identified as indicating brittle yielding, to date, no link has been established between all three phenomena, either experimentally or theoretically. The lack of a comprehensive understanding of the relationship between these three phenomena presents a significant challenge in predicting the mechanical behavior of YSFs under different conditions.

In this work, we provide a unified understanding of the variation in ductile and brittle yielding processes observed in different materials in a comparative manner. To maintain consistency with solid mechanics studies of failure mechanisms, we define a soft material as being more brittle than another if it undergoes a smaller amount of plastic deformation before yielding. To describe the variation in ductile and brittle yielding, we introduce a single parameter, which we call the brittility factor, to a continuum model that unifies the rheological physics above and below the yield stress by allowing elastic strain to enhance plastic strains. Within our model, the brittility factor modifies the contribution of rapid elastic deformation to the acquisition of plastic strain. We demonstrate its ability to accurately describe the behavior of a variety of YSFs with different microstructures, including gels and glasses, across a range of protocols. Our findings provide a practical approach to quantifying the brittleness of YSFs by creating a spectrum of ductile and brittle behaviors.

At a continuum level, it is common to model the yielding transition as an abrupt transition in terms of a critical yield stress, below which it is assumed no plastic flow occurs. The preyielding solid behavior is often described by different physics than the flowing state, a concept known as the Oldroyd–Prager formalism (97–100). A recently proposed model by Kamani, Donley, and Rogers (101), which we refer to as the KDR model, consists of a single differential equation that accounts for the linear and nonlinear rheology of model YSFs. The 1D version of the model is

$$\sigma + \lambda(\dot{\gamma})\dot{\sigma} = (\eta_f)\left(\dot{\gamma} + \frac{\eta_s}{G}\ddot{\gamma}\right), \quad [1]$$

where G is the elastic modulus, η_s is the structural viscosity, η_f is the flow viscosity, and $\lambda(\dot{\gamma})$ is the rate-dependent relaxation time that is a result of combining the recoverable and unrecoverable components,

$$\lambda(\dot{\gamma}) = \frac{\eta_f + \eta_s}{G} = \frac{\frac{\sigma_y}{|\dot{\gamma}|} + k|\dot{\gamma}|^{n-1} + \eta_s}{G}. \quad [2]$$

In the KDR model, the viscosity related to unrecoverable plastic deformation, which we call the flow viscosity, η_f, depends on the total strain rate, which includes the rate at which strain is acquired recoverably, $\dot{\gamma}(t) = \dot{\gamma}_{\text{rec}}(t) + \dot{\gamma}_{\text{unrec}}(t)$. Rapid elastic deformation therefore enhances plastic rearrangement by decreasing the flow viscosity. This formulation implies nonlocal physics. At the bulk scale, the model can acquire both elastic and plastic strains simultaneously, but at a local level, the strains must be mutually exclusive. That is, at any instant, mesoscopic elements like glassy cages can only deform recoverably or unrecoverably, but not both at the same time (102–104). The elastic straining elements must therefore be spatially separated from the elements deforming plastically. The enhancement of plastic strain by rapid elastic strain therefore implies nonlocal physics.

The formulation of the KDR model such that the elastic deformation assists in plastic rearrangements allows it to capture the transient behavior observed in a range of ductile YSFs. The model predicts the rate dependence of experimentally observed yield strains in steady shear startup, and transient creep and avalanche behaviors, as well as the gradual overshoot in the loss modulus seen in amplitude sweeps. However, there are more brittle YSFs that show stress overshoots in steady shear startup tests, delayed yielding in creep experiments, and steeper overshoots in the loss modulus during amplitude sweeps than are predicted by the KDR model. Experimentally, the difference in oscillatory behavior has been shown to occur due to rapid changes in unrecoverable processes (79), suggesting that the amount by which elastic deformation contributes to plastic rearrangement differs between materials.

We account for brittle behaviors by modifying the KDR model to allow for variance in the contribution to plastic deformation from elastic deformation using a parameter Bt, which we call the brittility factor. With the addition of the brittility factor to the KDR model, the flow viscosity that dictates how unrecoverable deformation is acquired, and the rate-dependent relaxation time shown in Eq. **2** become,

$$\eta_f = \frac{\sigma_y}{\left|\frac{\dot{\gamma}_{\text{rec}}}{Bt} + \dot{\gamma}_{\text{unrec}}\right|} + k\left|\frac{\dot{\gamma}_{\text{rec}}}{Bt} + \dot{\gamma}_{\text{unrec}}\right|^{n-1} = \frac{\sigma_y}{|\dot{\gamma}_{\text{eff}}|} + k\,|\dot{\gamma}_{\text{eff}}|^{n-1}, \quad [3]$$

and

$$\lambda(\dot{\gamma}) = \frac{\frac{\sigma_y}{|\frac{\dot{\gamma}_{rec}}{Bt}+\dot{\gamma}_{unrec}|} + k|\frac{\dot{\gamma}_{rec}}{Bt} + \dot{\gamma}_{unrec}|^{n-1} + \eta_s}{G}. \quad [4]$$

A full tensorial version of the brittility model is presented in *SI Appendix*. Inclusion of the brittility factor affects the rate that governs the plastic flow behavior, which we refer to as the effective shear rate $\dot{\gamma}_{eff} = \dot{\gamma}_{rec}/Bt + \dot{\gamma}_{unrec}$. If the brittility factor is one, $Bt = 1$, then the effective shear rate is simply the applied shear rate. However, if the brittility factor is greater than one, then the effective shear rate in a transient experiment where both recoverable and unrecoverable strain is being acquired is smaller than the applied shear rate. The reduction in effective shear rate means that the flow viscosity is larger than the case of a ductile response with a brittility factor of one. Larger brittility factors, therefore, result in smaller amounts of plastic deformation occurring under otherwise identical transient conditions.

Results and Discussion

In the main manuscript, our primary focus is on illustrating how the brittility parameter enables us to effectively capture the behavior of real materials across various test protocols. In *SI Appendix*, we display the effect of systematically varying the brittility factor while keeping the other five model parameters constant.

Given that our brittility factor represents a modification of the contribution to plastic deformation from rapid elastic deformation, we propose that Bt represents a separation of mechanical responses over different length scales and that Bt represents the ratio of some mesoscopic local modulus to the bulk modulus, $Bt = G_{local}/G_{bulk}$. The brittility factor in our model is similar to the cooperativity length that has been used in fluidity models, which quantifies the spatial spreading of plastic activity due to nonlocal elastic deformation (105–107). If both the local and bulk moduli are similar, then the brittility factor is close to one, and a ductile response is observed. In this case, the local structure deforms as much as the bulk and rapid elastic deformation fully contributes to plastic rearrangement. However, if the local structure is stiffer than the bulk, these local structures will deform less and be less able to propagate a strain field that will promote plastic activity to other parts of the material, and Bt becomes large. When $Bt \to \infty$, the local modulus restricts deformation, which means there is no mechanism for a gradual or ductile yielding transition and stress builds up until a more abrupt brittle yielding event occurs. Intermediate values of Bt between these extremes indicate the extent of brittleness. When determining the local modulus for the brittility factor, the length scale of individual particles becomes relevant (23, 80, 108). Philosophically, it may be more attractive to refer to the brittleness on a scale of zero to one as $1 - \frac{1}{Bt}$. In this case, a brittility factor of one means that ductile yielding is observed and the brittleness is zero. An infinite value of the brittility factor means the brittleness is one and the material is brittle.

Examination of Eq. **1** makes it clear that the large amplitude oscillatory shear (LAOS) protocol represents an ideal experimental scenario for testing and validating the model predictions (109). Although alternative protocols such as steady shear startup and creep tests are also employed to induce nonlinear behaviors, they do not probe the full constitutive relation and therefore present less stringent tests. In steady shear startup, the derivative of the strain rate remains zero, and in creep tests, the derivative of the stress remains zero. This means that the fourth and second terms of the constitutive relation shown in Eq. **1** are eliminated from the testing protocol, resulting in a less rigorous test of the whole model. In contrast, all the kinematic terms in Eq. **1** vary with time in the LAOS protocol and influence the predictions. LAOS therefore provides a more rigorous evaluation of the model's predictive capabilities. Consequently, our initial assessment focuses on testing the model predictions against both average and transient LAOS data.

The model can be completely parameterized experimentally. Two parameters are related to the way the model describes acquisition of recoverable strain and are determined from the linear viscoelastic response. Three parameters are related to the unrecoverable acquisition of strain and are determined from the steady-state flow curve. The brittility factor, which governs how recoverable and unrecoverable parts interact, can be determined either by using the reported value of local modulus measured using AFM or by fitting the model predictions to amplitude sweep data. In this work, once all six parameters have been determined in this manner, they are fixed and we then present predictions of the transient behaviors to LAOS, steady shear startup, and creep tests. Other metrics derived from these tests, including the size of the stress overshoots in LAOS and steady shear startup, and the timing of delayed yielding are shown for completeness in *SI Appendix*.

We show in Fig. 1 how accurately the model predicts the nonlinear rheology of a concentrated suspension of poly-isopropylacrylamide (PNiPAM) microgel particles from the work of van der Vaart et al. (108). In this case, the brittility factor is determined to be 50 from atomic force microscopy (AFM) measurements of the local modulus of the microgel particles and conventional rheometry to measure the bulk modulus. As a comparison, we also show predictions using $Bt = 1$. An alternative method to determine the brittility factor, when AFM or other localized data are unavailable, is by fitting the model predictions to a rheological response, including the amplitude sweep data.

In Fig. 2, we show a range of responses from 4 different materials under oscillatory shearing. The data are presented in the form of dynamic moduli, which physically represent the average energy stored and dissipated per cycle (110). The brittility model is able to account for the yielding behavior of each material, including the change in slope and the overshoot in the loss modulus. At small strain amplitudes, the moduli are independent of the strain amplitude, while both moduli decrease at the largest amplitudes. At intermediate amplitudes, an overshoot is observed in the loss modulus, the onset of which can either be gradual, as seen for Carbopol 980 with $Bt = 1$, or steep, as seen for the soft glass made of a suspension of star polymers with $Bt = 20$, concentrated Ludox with $Bt = 100$, and Xanthan gum with $Bt = 1{,}000$. The steepness of the onset of the increase in the loss modulus is accurately captured by the model with different values of the brittility factor. The decreased effective shear rate with increasing brittility leads to a longer relaxation time, which in turn results in more solid-like behavior at intermediate strain amplitudes. The loss modulus therefore does not begin increasing until larger amplitudes are applied. The extended linear regime for more brittle materials has been reported as a design criterion for inks to be used in direct ink writing (81). At the largest strain amplitudes, the unrecoverable deformation is much larger than the recoverable deformation, and the term $\dot{\gamma}_{rec}/Bt$ contributes less to the flow viscosity, as evident from Eq. **3**. The highest rate behaviors are therefore similar.

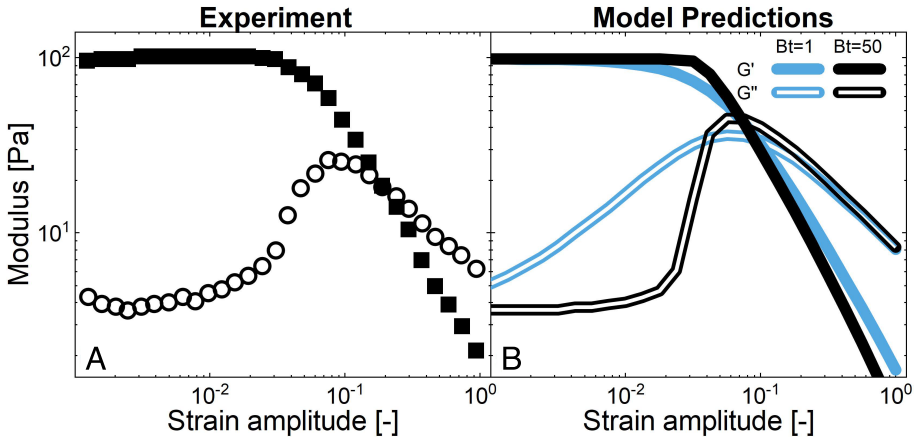

Fig. 1. Comparison of the dynamic moduli $G'(\gamma_0)$ and $G''(\gamma_0)$ between the experimental data (*A*) and the KDR model (*B*) with the brittility factor of $Bt = G_{local}/G_{bulk} = 50$, for suspension of poly-isopropylacrylamide (PNiPAM) microgel particles. The local modulus was determined using AFM. The model accurately predicts the degree of steepness observed in the overshoot of the loss modulus. Blue lines show model predictions with a brittility factor of $Bt = 1$. Model parameters are listed in *SI Appendix*. Experimental data were taken from ref. 108.

Having determined the brittility factor by fitting model predictions to the amplitude sweep behavior, and having already determined the values of the remaining five parameters from the frequency sweep and steady shear flow curve, we now keep all parameters fixed and predict the transient behaviors. Although the model accurately predicts the average response of the dynamic moduli as seen in Fig. 2, a more rigorous assessment of the model's validity and applicability can be conducted by analyzing the transient LAOS responses. This can be achieved by comparing the Lissajous curves, in which the stress is plotted parametrically against the total strain from an entire period, as shown in Fig. 3. The model captures all of the features observed experimentally, including the overall shape of the waveforms, as well as the instantaneous slopes of the curves in different regions. This includes stress overshoots near the strain extrema observed for the soft glass made of a suspension of colloidal star polymers. The peak of the stress overshoot has been referred to as the static yield stress and is often interpreted as the stress that must be overcome for flow to initiate. We show in *SI Appendix* that our model predicts the same power-law increase in static yield stress at large strain amplitudes, as observed in the experiments. Because stress overshoots in particular have been associated with brittle yielding, it is worth understanding how the model accounts for them. The local extremum of the stress is found by substituting $\dot{\sigma} = 0$ and $\ddot{\gamma} = -\omega^2\gamma$ into Eq. **1** and solving for the stress,

$$\sigma = \eta_f\left(\dot{\gamma} + \frac{\eta_s}{G}\ddot{\gamma}\right) = \left(\frac{\sigma_y}{\left|\frac{\dot{\gamma}_{rec}}{Bt} + \dot{\gamma}_{unrec}\right|} + k\left|\frac{\dot{\gamma}_{rec}}{Bt} + \dot{\gamma}_{unrec}\right|^{n-1}\right)\left(\dot{\gamma} - \frac{\eta_s}{G}\omega^2\gamma\right). \quad [5]$$

If the brittility factor is one, $Bt = 1$, then the applied shear rate $\dot{\gamma}$ and the effective shear rate governing the plastic flow behavior are equal. However, the effective shear rate is smaller than the applied shear rate for a material with a brittility factor

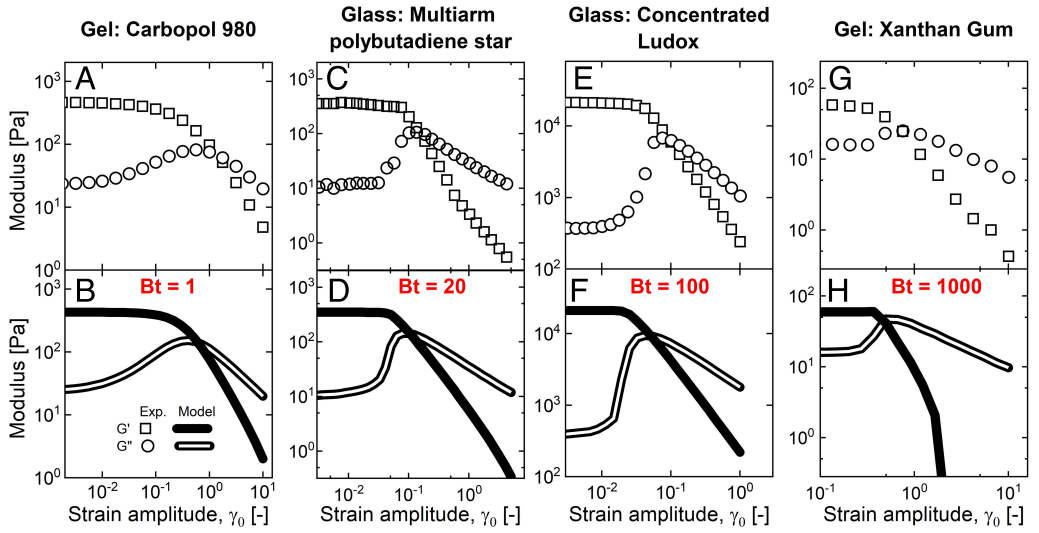

Fig. 2. Comparison of the dynamic moduli $G'(\gamma_0)$ and $G''(\gamma_0)$ between the experimental data and the KDR model with the brittility factor for Carbopol 980 (*A* and *B*), multiarm polybutadiene star (*C* and *D*), concentrated Ludox (*E* and *F*), and xanthan gum (*G* and *H*). The value of the brittility factor for each YSF is denoted in red text. The model accurately predicts the degree of steepness observed in the overshoot of the loss modulus for all YSFs. Model parameters are listed in *SI Appendix*.

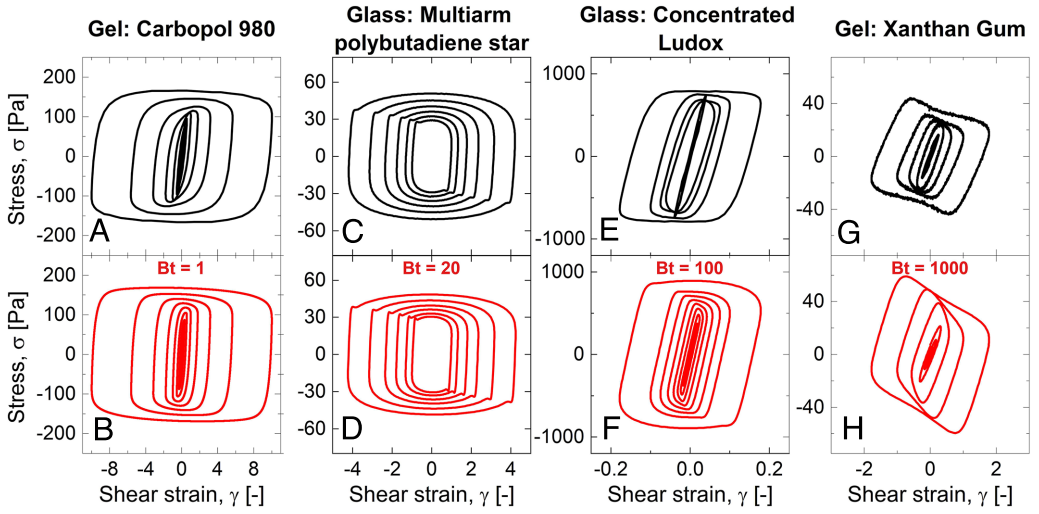

Fig. 3. Comparison of the elastic Lissajous curves from the amplitude sweep at $\omega = 1$ rad/s, between experiments and model predictions for Carbopol 980 (*A* and *B*), multiarm polybutadiene star (*C* and *D*), concentrated Ludox (*E* and *F*) and xanthan gum (*G* and *H*). The model predictions are shown in red, and model parameters are listed in *SI Appendix*.

greater than one, such as the soft glass of colloidal star polymers. The smaller effective shear rate leads to a higher flow viscosity, η_f resulting in smaller amounts of unrecoverable strain being acquired for a given stress and an increased elastic response. The smaller effective shear rate and larger flow viscosity mean that the recoverable strain continues to grow to be larger than the flowing case, which we call overstretching. This overstretching leads to the stress overshoots, as shown in more detail in *SI Appendix*.

The model's ability to accurately predict the transient behavior of the different YSFs indicates its effectiveness in capturing the underlying physics of the yielding transition at a level that is independent of microstructural information.

To display how brittleness affects the yielding transition during oscillatory shear, we plot the rates at which strain is acquired unrecoverably and recoverably against each other in Fig. 4. The shaded region indicates when the recoverable rate is higher, and the unshaded region indicates when the unrecoverable rate is higher. This presentation allows us to determine how and when yielding takes place. The model response changes from acquiring strain recoverably to unrecoverably based on the kinematics, rather than a particular value of the stress or a feature in the evolution of the stress (111). In Fig. 4, we show the effect of varying the brittility factor by 100 while keeping other parameters constant, on an oscillatory shear test with an applied strain amplitude of 10 strain units and angular frequency of 1 rad/s. The component rate Lissajous curves are shown in Fig. 4 *A* and *C*, and the corresponding traditional elastic Lissajous curves are shown in Fig. 4 *B* and *D*. For a ductile response, where the brittility factor is one, the model predicts a sequence of four distinct behaviors corresponding to elastic deformation, yielding, plastic flow, and unyielding. The same four processes have been reported experimentally for a number of systems (108, 111–118). However, as the response becomes more brittle and the brittility factor becomes larger than one, the model exhibits overstretching, which is characterized by a higher maximum recoverable rate compared to the case of a ductile material. Yielding then occurs at a faster rate than is observed for more ductile materials, as indicated by the shallower slope of the unrecoverable vs recoverable rate curve for process two in Fig. 4 *A* and *C*. Following this rapid yielding, an additional distinct process of recoil takes place, where the recoverable rate is negative while the unrecoverable rate remains positive (119–121). The overstretching and subsequent recoil appears as a stress overshoot, as seen in the traditional elastic Lissajous curve, as shown in Fig. 4*D*.

Given that the responses of YSFs have been studied under a variety of protocols, it is important to see the model predictions for the same experiments. In Fig. 5, we compare the model predictions to experimental data from steady shear startup and creep experiments on the soft glass made of a concentrated suspension of colloidal star polymers. While the predictions of the responses to these protocols act as an excellent test because of the difference in kinematics, they are less rigorous tests than LAOS because they do not probe all terms of the constitutive model. Having established the ability of the model to describe the LAOS rheology, we keep all parameters the same and show its accuracy in predicting the steady shear startup and creep responses. When determining the model response, the initial conditions for the steady shear startup and creep tests were matched with those observed experimentally. This is necessary because the preshear protocol employed left the system in a reproducible but not completely relaxed nor isotropic condition (122, 123). Details can be found in *SI Appendix*.

During steady shear startup tests, at early times across a range of imposed shear rates, an elastic solid-like response leads to a linear increase in the stress. At long times, the material has yielded and is flowing plastically, with the stress taking the steady-state value. The process of yielding determines the path between these two states. At intermediate times for small imposed shear rates, gradual transitions in the stress response with no overshoots are observed. However, at intermediate and higher shear rates, a distinct stress overshoot becomes evident. Our model with a brittility factor greater than one predicts the same rate-dependent stress overshoot responses. At small imposed shear rates, the imposed shear rate and the effective shear rate are almost the same. This means the imposed kinematics are extremely slow, preventing the material from overstretching. At higher rates, the model predicts a stress overshoot via the causes identified earlier: The smaller effective shear rate that leads to an increased elastic response and overstretching. An example is also shown in *SI Appendix* for steady shear startup. The dependence of the size of the stress overshoot on the applied shear rate has been

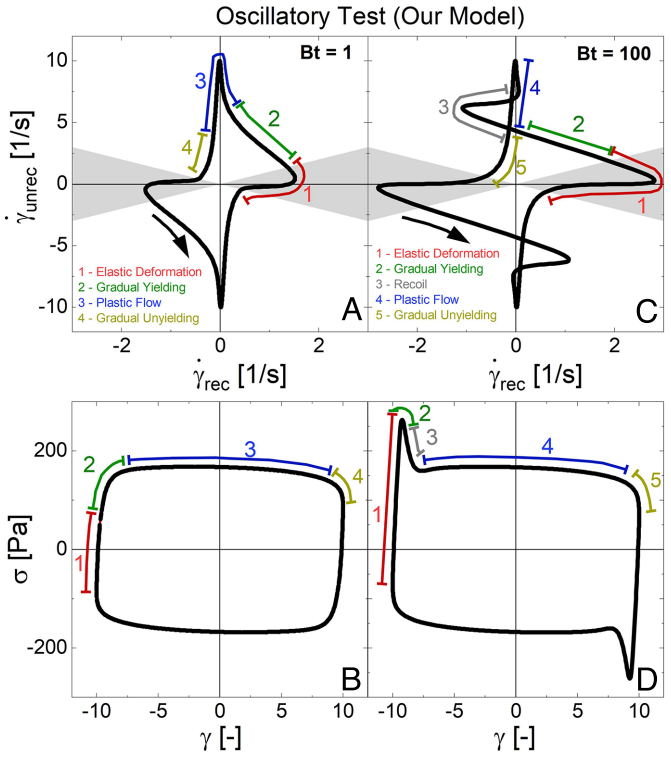

Fig. 4. Comparison of the time-resolved strain decomposition analysis for our model with brittility factor at $\gamma = 10$ [-] strain units for two cases: ductile ($Bt = 1$) and brittle ($Bt = 100$). All the model parameters except the brittility factor are kept constant. The analysis results are presented using two types of Lissajous curves: (*A* and *C*) a component rate Lissajous curve and (*B* and *D*) a traditional "elastic" Lissajous curve. The black arrows indicate the trajectory direction, and the numbers indicate the distinct transitions observed in the ductile and brittle cases, as discussed in the accompanying text.

previously reported (42, 49, 100, 124, 125). In *SI Appendix*, we demonstrate that our model predicts the same power-law increase in the size of the overshoot with increasing shear rates as observed in the experiments. No stress overshoot is observed for ductile materials, such as the Carbopol 980, as shown in the *Inset* of Fig. 5*B*, in *SI Appendix*, and in ref. 101. For such ductile materials, the effective shear rate will always be equal to the applied shear rate, preventing overstretching.

We have shown that our brittility model predicts stress overshoots in LAOS and steady-shear start-up experiments. The peak stress has often been reported as the static yield stress, beyond which flow begins (49, 108, 112, 118). In *SI Appendix*, we show that our model predicts the same power-law increase as observed in both experimental protocols with the same model parameters as determined earlier. At steady-state, the model follows the Herschel–Bulkley flow curve with a dynamic yield stress, σ_y, below which stable flow ceases. Our brittility model accounts for both behaviors with only a single yield stress in the constitutive behavior. It may therefore be generally true that static and dynamic yielding are manifestations of the complex kinematics of the experimental protocol acting on a constitutive relation that has a single yield stress. While they present distinct phenomena, their underlying cause can be understood in terms of the same physics.

During creep tests in which a constant shear stress is applied, the viscosity has been observed to bifurcate about the yield stress at long times. Stresses larger than the yield stress often induce avalanche behavior after some delay. We compare results from creep experiments on colloidal star glasses and the predictions of the brittility model in Fig. 5 *C* and *D*, showing that the model predicts delayed yielding. The creep response of the model can be determined by substituting $\dot{\sigma} = 0$ into Eq. **1** and solving for the evolution of the strain rate,

$$\ddot{\gamma} = \left(\frac{\sigma}{\left(\frac{\sigma_y}{\left| \frac{\dot{\gamma}_{\text{rec}}}{Bt} + \dot{\gamma}_{\text{unrec}} \right|} + k \left| \frac{\dot{\gamma}_{\text{rec}}}{Bt} + \dot{\gamma}_{\text{unrec}} \right|^{n-1} \right)} - \dot{\gamma} \right) \frac{G}{\eta_s}. \quad [6]$$

The underlying physics that allows the model to predict delayed yielding behavior for $Bt > 1$ can be understood by breaking the response down into distinct regions, the first of which is the initial response where the strain rate drops and no flow is taking place. Substituting $\dot{\gamma}_{\text{unrec}} \approx 0$ into Eq. **6** gives,

$$\ddot{\gamma} = \left(\frac{\sigma}{Bt\sigma_y + Bt^{1-n} k |\dot{\gamma}_{\text{rec}}|^n} - 1 \right) \frac{G\dot{\gamma}_{\text{rec}}}{\eta_s}. \quad [7]$$

The rate at which the strain rate changes will be negative if the fraction in the brackets of Eq. **7** is less than one, making the denominator an effective yield stress. Initially, when all strain is acquired recoverably, the effective yield stress is larger than the equilibrium value by a factor proportional to Bt. Therefore, for stresses greater than the equilibrium yield stress but less than the effective yield stress, $\sigma_y < \sigma \leq \sigma_{y,\text{eff}}$, a brittle material won't yield immediately, and the strain rate will drop. As the recoverable strain saturates and its rate of acquisition goes to zero, $\dot{\gamma}_{\text{rec}} \to 0$, the model's behavior undergoes a significant transition, characterized by a steep increase in the total strain rate with time, before reaching the steady state value. Substituting $\dot{\gamma}_{\text{rec}} = 0$ into Eq. **6** results in,

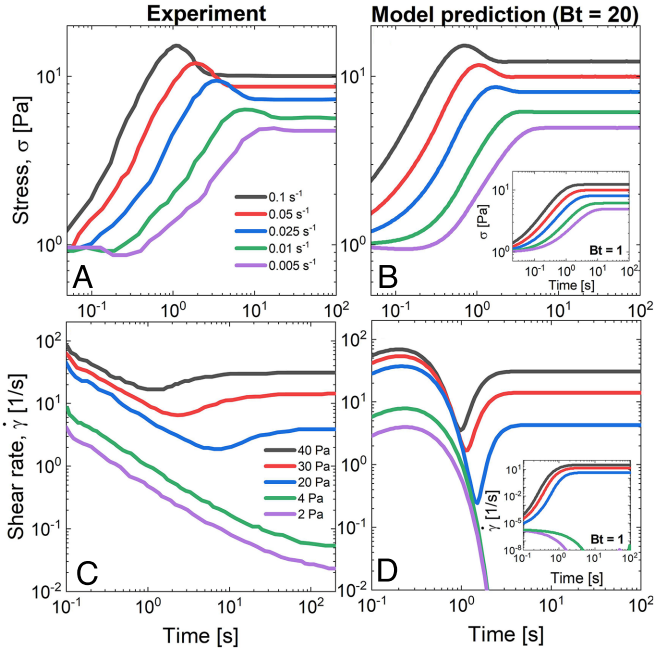

Fig. 5. Comparison of the experiment (*A*) and model (*B*) predictions for steady shear startup test at various applied shear rates for multiarm polybutadiene star polymers. The *Inset* in (*B*) shows the model results for the brittility factor $Bt = 1$. Comparison of the experiment (*C*) and model results (*D*) for steady creep tests at various applied stress magnitudes. The *Inset* in (*D*) shows the model results for the brittility factor $Bt = 1$. Model parameters are listed in *SI Appendix*.

$$\ddot{\gamma} = \left(\frac{\sigma}{\sigma_y + k|\dot{\gamma}_{unrec}|^n} - 1 \right) \frac{G\dot{\gamma}_{unrec}}{\eta_s}. \quad [8]$$

Having previously been larger by a factor proportional to Bt, when the recoverable strain rate drops, the effective yield stress also drops back down to the equilibrium value σ_y. If the applied stress is held constant above the equilibrium yield stress, the strain rate will therefore eventually increase exponentially until it reaches the steady state. The model therefore predicts delayed yielding when the brittility factor is greater than one and when the applied stress is less than the effective yield stress but greater than the equilibrium value, as shown in Fig. 5*D*. As demonstrated in *SI Appendix* and the *Inset* of Fig. 5*D*, no delayed yielding is observed in ductile materials like Carbopol 980 (101), where the brittility factor is one and the effective yield stress remains fixed at the equilibrium value σ_y. We show in *SI Appendix* that our model also predicts a power-law decrease in fluidization time with increasing applied shear stress.

We have demonstrated a degree of universality in the spectrum of yielding behaviors observed in soft materials by introducing the brittility factor to a continuum elastoviscoplastic model. We have treated the brittility factor as a material constant and have shown, using the data of van der Vaart et al. (108), that AFM measurements can be used to determine the local modulus, and therefore, the brittility factor, providing a method to determine all model parameters experimentally. The utility of the framework allows the comparison of YSFs as being ductile or brittle relative to one another. Our model accounts for a range of yielding behaviors by modifying the contribution of the recoverable strain to the plastic deformation, which impacts the rate at which yielding occurs and the amount of recoverable strain acquired prior to yielding. Therefore, the brittility factor affects how the material yields without affecting the steady state where strain is only acquired unrecoverably. Our model predicts phenomena observed in a variety of flow protocols, and we have shown that they can all be described with the addition of a single parameter that indicates how far along the spectrum a material sits. Brittility in the sense we have used it here accounts for, or controls, the amount of plastic deformation acquired before yielding, as determined by the steepness of the overshoot in the loss modulus observed in amplitude sweeps, the size and rate dependence of stress overshoots in steady shear startup and LAOS responses, as well as delayed yielding in creep tests. The brittility factor, therefore, brings all of these phenomena under the same umbrella and, through its interpretation as a ratio of a local to a bulk modulus, provides a possible design criterion for the creation of new soft materials with specified rheology.

Materials and Methods

We compare the prediction from the model obtained numerically using MATLAB, to experimental rheological data collected from a simple YSF: a polymer microgel–Carbopol 980, 1 wt% (*SI Appendix*); a biopolymer suspension–Xanthan gum, 4 wt%; a dense (glassy) colloidal suspension–concentrated Ludox TM-50, 42 vol%; and a multiarm polybutadiene star polymer system. The details regarding rheological geometries and where the rheological data were taken can be found in *SI Appendix*.

Measurements for Carbopol 980, Xanthan gum, and concentrated Ludox were made with Anton Paar Modular Compact Rheometer (MCR) 302e and 702. Their synchronous motor allows for experiments to be conducted in strain-controlled and stress-controlled modes.

For each material, Linear-regime frequency sweeps were used to obtain the model parameters related to recoverable components of the model, with G and η_s determined from the frequency-independent $G = G'$ and $\eta_s = G''$, ω=1 rad/s. The steady shear flow curve is fit by the Herschel–Bulkley model. The brittility factor was determined from fitting to amplitude sweep for various materials. Model parameter values for all materials are listed in *SI Appendix*.

Data, Materials, and Software Availability. All study data presented in the manuscript are available in the Mendeley Data repository (126). All other study data are included in the article and/or *SI Appendix*.

ACKNOWLEDGMENTS. We thank Anton Paar for the use of the TwinDrive MCR 702 through their academic program. This material is based upon work supported by NSF Grant 1847389.

1. J. M. Ginder, L. Davis, L. Elie, Rheology of magnetorheological fluids: Models and measurements. *Int. J. Mod. Phys. B.* **10**, 3293–3303 (1996).
2. X. Liu *et al.*, Synthesis and electrorheological properties of polar molecule-dominated TiO_2 particles with high yield stress. *Rheol. Acta* **49**, 837–843 (2010).
3. Y. D. Liu, H. J. Choi, Electrorheological fluids: Smart soft matter and characteristics. *Soft Matter* **8**, 11961–11978 (2012).
4. W. Mickel *et al.*, Robust pore size analysis of filamentous networks from three-dimensional confocal microscopy. *Biophys. J.* **95**, 6072–6080 (2008).
5. A. R. Patel, M. D. Bora Mankoč, B. Sintang, A. Lesaffer, K. Dewettinck, Fumed silica-based organogels and 'aqueous-organic' bigels. *RSC Adv.* **5**, 9703–9708 (2015).
6. H. J. Walls, S. Brett Caines, A. M. Sanchez, S. A. Khan, Yield stress and wall slip phenomena in colloidal silica gels. *J. Rheol.* **47**, 847–868 (2003).
7. H.-G. Yang, C.-Z. Li, G. Hong-Chen, T.-N. Fang, Rheological behavior of titanium dioxide suspensions. *J. Colloid Interface Sci.* **236**, 96–103 (2001).
8. D. J. Klingenberg, C. F. Zukoski IV, Studies on the steady-shear behavior of electrorheological suspensions. *Langmuir* **6**, 15–24 (1990).
9. H. Daniel Bonn, G. W. Tanaka, H. Kellay, J. Meunier, Aging of a colloidal 'wigner' glass. *Europhys. Lett.* **45**, 52 (1999).
10. D. Bonn, M. M. Denn, Yield stress fluids slowly yield to analysis. *Science* **324**, 1401–1402 (2009).
11. A. Burmistrova, R. von Klitzing, Control of number density and swelling/shrinking behavior of P(NIPAM-AAc) particles at solid surfaces. *J. Mater. Chem.* **20**, 3502–3507 (2010).
12. C. Clasen, B. P. Gearing, G. H. McKinley, The flexure-based microgap rheometer (FMR). *J. Rheol.* **50**, 883–905 (2006).
13. M. Cloitre, R. Borrega, F. Monti, L. Leibler, Glassy dynamics and flow properties of soft colloidal pastes. *Phys. Rev. Lett.* **90**, 068303 (2003).
14. M. Jalaal, G. Cottrell, N. Balmforth, B. Stoeber, On the rheology of pluronic f127 aqueous solutions. *J. Rheol.* **61**, 139–146 (2017).
15. T. Jiang, C. F. Zukoski, Rheology of high density glass of binary colloidal mixtures in unentangled polymer melts. *Soft Matter* **9**, 3117–3130 (2013).
16. R. C. Kramb, C. F. Zukoski, Nonlinear rheology and yielding in dense suspensions of hard anisotropic colloids. *J. Rheol.* **55**, 1069–1084 (2011).
17. M. Le Merrer, R. Lespiat, R. Höhler, S. Cohen-Addad, Linear and non-linear wall friction of wet foams. *Soft Matter* **11**, 368–381 (2015).
18. K. N. Nordstrom *et al.*, Microfluidic rheology of soft colloids above and below jamming. *Phys. Rev. Lett.* **105**, 175701 (2010).
19. C. S. O'Bryan *et al.*, Self-assembled micro-organogels for 3D printing silicone structures. *Sci. Adv.* **3**, e1602800 (2017).
20. J.-M. Piau, Carbopol gels: Elastoviscoplastic and slippery glasses made of individual swollen sponges: Meso-and macroscopic properties, constitutive equations and scaling laws. *J. Nonnewton. Fluid Mech.* **144**, 1–29 (2007).
21. S. A. Rogers, B. M. Erwin, D. Vlassopoulos, M. Cloitre, Oscillatory yielding of a colloidal star glass. *J. Rheol.* **55**, 733–752 (2011).
22. H. Senff, W. Richtering, Temperature sensitive microgel suspensions: Colloidal phase behavior and rheology of soft spheres. *J. Chem. Phys.* **111**, 1705–1711 (1999).
23. T. Jiang, C. F. Zukoski, Role of particle size and polymer length in rheology of colloid–polymer composites. *Macromolecules* **45**, 9791–9803 (2012).
24. P. Bertsch, M. Diba, D. J. Mooney, S. C. G. Leeuwenburgh, Self-healing injectable hydrogels for tissue regeneration. *Chem. Rev.* **123**, 834–873 (2022).
25. A. K. Grosskopf *et al.*, Viscoplastic matrix materials for embedded 3D printing. *ACS Appl. Mater. Interfaces* **10**, 23353–23361 (2018).
26. M. Schaffner, P. A. Rühs, F. Coulter, S. Kilcher, A. R. Studart, 3D printing of bacteria into functional complex materials. *Sci. Adv.* **3**, eaao6804 (2017).
27. A. H. Williams *et al.*, Printable homocomposite hydrogels with synergistically reinforced molecular-colloidal networks. *Nat. Commun.* **12**, 1–9 (2021).
28. P. Wei *et al.*, Go with the flow: Rheological requirements for direct ink write printability. *J. Appl. Phys.* **134**, 100701 (2023).
29. D. Bonn, M. M. Denn, L. Berthier, T. Divoux, S. Manneville, Yield stress materials in soft condensed matter. *Rev. Mod. Phys.* **89**, 035005 (2017).
30. M. A. Meyers *et al.*, Structural biological composites: An overview. *JOM* **58**, 35–41 (2006).
31. F. Barthelat, Z. Yin, M. J. Buehler, Structure and mechanics of interfaces in biological materials. *Nat. Rev. Mater.* **1**, 1–16 (2016).
32. H. Peterlik, P. Roschger, K. Klaushofer, P. Fratzl, From brittle to ductile fracture of bone. *Nat. Mater.* **5**, 52–55 (2006).
33. P. Schall, D. A. Weitz, F. Spaepen, Structural rearrangements that govern flow in colloidal glasses. *Science* **318**, 1895–1899 (2007).
34. W. D. Callister, D. G. Rethwisch, *Materials Science and Engineering: An Introduction* (Wiley, New York, NY, 1964).

35. A. H. Cottrell, *The Mechanical Properties of Matter* (Krieger Publishing, 1964).
36. F. Célarié *et al*., Glass breaks like metal, but at the nanometer scale. *Phys. Rev. Lett.* **90**, 075504 (2003).
37. T. Divoux, D. Tamarii, C. Barentin, S. Manneville, Transient shear banding in a simple yield stress fluid. *Phys. Rev. Lett.* **104**, 208301 (2010).
38. T. Gibaud, C. Barentin, S. Manneville, Influence of boundary conditions on yielding in a soft glassy material. *Phys. Rev. Lett.* **101**, 258302 (2008).
39. J.-S. Lee, Y.-S. Kim, K.-W. Song, Transient rheological behavior of natural polysaccharide *Xanthan* gum solutions in start-up shear flow fields: An experimental study using a strain-controlled rheometer. *Kor.-Austr. Rheol. J.* **27**, 227–239 (2015).
40. B. Keshavarz, T. Divoux, S. Manneville, G. H. McKinley, Nonlinear viscoelasticity and generalized failure criterion for polymer gels. *ACS Macro Lett.* **6**, 663–667 (2017).
41. J. Colombo, E. Del Gado, Stress localization, stiffening, and yielding in a model colloidal gel. *J. Rheol.* **58**, 1089–1116 (2014).
42. T. Divoux, C. Barentin, S. Manneville, Stress overshoot in a simple yield stress fluid: An extensive study combining rheology and velocimetry. *Soft Matter* **7**, 9335–9349 (2011).
43. T. Divoux, D. Tamarii, C. Barentin, S. Teitel, S. Manneville, Yielding dynamics of a Herschel–Bulkley fluid: A critical-like fluidization behaviour. *Soft Matter* **8**, 4151–4164 (2012).
44. N. Koumakis, A. Pamvouxoglou, A. S. Poulos, G. Petekidis, Direct comparison of the rheology of model hard and soft particle glasses. *Soft Matter* **8**, 4271–4284 (2012).
45. C. P. Amann *et al*., Overshoots in stress–strain curves: Colloid experiments and schematic mode coupling theory. *J. Rheol.* **57**, 149–175 (2013).
46. V. Carrier, G. Petekidis, Nonlinear rheology of colloidal glasses of soft thermosensitive microgel particles. *J. Rheol.* **53**, 245–273 (2009).
47. F. Khabaz, B. F. Di Dio, M. Cloitre, R. T. Bonnecaze, Transient dynamics of soft particle glasses in startup shear flow. Part I: Microstructure and time scales. *J. Rheol.* **65**, 241–255 (2021).
48. L. Cipelletti, K. Martens, L. Ramos, Microscopic precursors of failure in soft matter. *Soft Matter* **16**, 82–93 (2020).
49. C. Derec, G. Ducouret, A. Ajdari, F. Lequeux, Aging and nonlinear rheology in suspensions of polyethylene oxide-protected silica particles. *Phys. Rev. E* **67**, 061403 (2003).
50. R. Benzi *et al*., Continuum modeling of shear startup in soft glassy materials. *Phys. Rev. E* **104**, 034612 (2021).
51. H. J. Barlow, J. O. Cochran, S. M. Fielding, Ductile and brittle yielding in thermal and athermal amorphous materials. *Phys. Rev. Lett.* **125**, 168003 (2020).
52. M. Ozawa, L. Berthier, G. Biroli, A. Rosso, G. Tarjus, Random critical point separates brittle and ductile yielding transitions in amorphous materials. *Proc. Natl. Acad. Sci. U.S.A.* **115**, 6656–6661 (2018).
53. V. V. Vasisht, G. Roberts, E. Del Gado, Emergence and persistence of flow inhomogeneities in the yielding and fluidization of dense soft solids. *Phys. Rev. E* **102**, 010604 (2020).
54. V. V. Vasisht, E. Del Gado, Computational study of transient shear banding in soft jammed solids. *Phys. Rev. E* **102**, 012603 (2020).
55. M. Ozawa, L. Berthier, G. Biroli, G. Tarjus, Rare events and disorder control the brittle yielding of well-annealed amorphous solids. *Phys. Rev. Res.* **4**, 023227 (2022).
56. S. Rossi, G. Biroli, M. Ozawa, G. Tarjus, F. Zamponi, Finite-disorder critical point in the yielding transition of elastoplastic models. *Phys. Rev. Lett.* **129**, 228002 (2022).
57. M. Singh, M. Ozawa, L. Berthier, Brittle yielding of amorphous solids at finite shear rates. *Phys. Rev. Mater.* **4**, 025603 (2020).
58. R. Benzi *et al*., Continuum modeling of soft glassy materials under shear. *Europhys. Lett.* **141**, 56001 (2023).
59. P. Coussot, Q. D. Nguyen, H. T. Huynh, D. Bonn, Avalanche behavior in yield stress fluids. *Phys. Rev. Lett.* **88**, 175501 (2002).
60. J. H. Cho, I. Bischofberger, Yield precursor in primary creep of colloidal gels. *Soft Matter* **18**, 7612–7620 (2022).
61. P. H. T. Uhlherr *et al*., The shear-induced solid–liquid transition in yield stress materials with chemically different structures. *J. Nonnewton. Fluid Mech.* **125**, 101–119 (2005).
62. V. Grenard, T. Divoux, N. Taberlet, S. Manneville, Timescales in creep and yielding of attractive gels. *Soft Matter* **10**, 1555–1571 (2014).
63. T. Bauer, J. Oberdisse, L. Ramos, Collective rearrangement at the onset of flow of a polycrystalline hexagonal columnar phase. *Phys. Rev. Lett.* **97**, 258303 (2006).
64. J. Sprakel, S. B. Lindström, T. E. Kodger, D. A. Weitz, Stress enhancement in the delayed yielding of colloidal gels. *Phys. Rev. Lett.* **106**, 248303 (2011).
65. M. Siebenbürger, M. Ballauff, T. Voigtmann, Creep in colloidal glasses. *Phys. Rev. Lett.* **108**, 255701 (2012).
66. T. Sentjabrskaja *et al*., Creep and flow of glasses: Strain response linked to the spatial distribution of dynamical heterogeneities. *Sci. Rep.* **5**, 11884 (2015).
67. S. Aime, L. Ramos, L. Cipelletti, Microscopic dynamics and failure precursors of a gel under mechanical load. *Proc. Natl. Acad. Sci. U.S.A.* **115**, 3587–3592 (2018).
68. J. H. Cho, I. Bischofberger, Yield precursor in primary creep of colloidal gels. *Soft Matter* **18**, 7612–7620 (2022).
69. S. B. Lindström, T. E. Kodger, J. Sprakel, D. A. Weitz, Structures, stresses, and fluctuations in the delayed failure of colloidal gels. *Soft Matter* **8**, 3657–3664 (2012).
70. P. J. Skrzeszewska *et al*., Fracture and self-healing in a well-defined self-assembled polymer network. *Macromolecules* **43**, 3542–3548 (2010).
71. D. Bonn, H. Kellay, M. Prochnow, K. Ben-Djemiaa, J. Meunier, Delayed fracture of an inhomogeneous soft solid. *Science* **280**, 265–267 (1998).
72. M. Leocmach, C. Perge, T. Divoux, S. Manneville, Creep and fracture of a protein gel under stress. *Phys. Rev. Lett.* **113**, 038303 (2014).
73. K. Hyun, S. H. Kim, K. H. Ahn, S. J. Lee, Large amplitude oscillatory shear as a way to classify the complex fluids. *J. Nonnewton. Fluid Mech.* **107**, 51–65 (2002).
74. T. G. Mason, J. Bibette, D. A. Weitz, Elasticity of compressed emulsions. *Phys. Rev. Lett.* **75**, 2051 (1995).
75. T. G. Mason, D. A. Weitz, Linear viscoelasticity of colloidal hard sphere suspensions near the glass transition. *Phys. Rev. Lett.* **75**, 2770 (1995).
76. T. G. Mason, M.-D. Lacasse, G. S. Grest, J. Dov Levine, Bibette, and DA Weitz., Osmotic pressure and viscoelastic shear moduli of concentrated emulsions. *Phys. Rev. E* **56**, 3150 (1997).
77. A. R. Payne, The dynamic properties of carbon black-loaded natural rubber vulcanizates. Part I. *J. Appl. Polym. Sci.* **6**, 57–63 (1962).
78. H. M. Wyss *et al*., Strain-rate frequency superposition: A rheological probe of structural relaxation in soft materials. *Phys. Rev. Lett.* **98**, 238303 (2007).
79. G. J. Donley, P. K. Singh, A. Shetty, S. A. Rogers, Elucidating the G'' overshoot in soft materials with a yield transition via a time-resolved experimental strain decomposition. *Proc. Natl. Acad. Sci. U.S.A.* **117**, 21945–21952 (2020).
80. S. Gupta *et al*., Advanced rheological characterization of soft colloidal model systems. *J. Phys.: Condens. Matter* **24**, 464102 (2012).
81. A. Corker, H.C.-H. Ng, R. J. Poole, E. García-Tuñón, 3D printing with 2D colloids: Designing rheology protocols to predict 'printability' of soft-materials. *Soft Matter* **15**, 1444–1456 (2019).
82. T. G. Mezger, *The Rheology Handbook: For Users of Rotational and Oscillatory Rheometers* (Vincentz Network GMBH & Co., Hannover, Germany, 2006).
83. T. Savouré, M. Dornier, L. Vachoud, A. Collignan, Clustering of instrumental methods to characterize the texture and the rheology of slimy okra (*Abelmoschus esculentus*) suspensions. *J. Texture Stud.* **51**, 426–443 (2020).
84. J. Thomas *et al*., Mechanical integrity in a dynamic interpenetrating hydrogel network of supramolecular peptide-polysaccharide supports enhanced chondrogenesis. *ACS Biomater. Sci. Eng.* **7**, 5798–5809 (2021).
85. T. N. Ofei, B. Lund, A. Saasen, S. Sangesland, The effect of oil–water ratio on rheological properties and sag stability of oil-based drilling fluids. *J. Energy Res. Technol.* **144**, 073008 (2022).
86. D. Alatalo, F. Hassanipour, An experimental study on human milk rheology: Behavior changes from external factors. *Fluids* **5**, 42 (2020).
87. G. P. Shrivastav, P. Chaudhuri, J. Horbach, Yielding of glass under shear: A directed percolation transition precedes shear-band formation. *Phys. Rev. E* **94**, 042605 (2016).
88. G. Parisi, I. Procaccia, C. Rainone, M. Singh, Shear bands as manifestation of a criticality in yielding amorphous solids. *Proc. Natl. Acad. Sci. U.S.A.* **114**, 5577–5582 (2017).
89. P. Urbani, F. Zamponi, Shear yielding and shear jamming of dense hard sphere glasses. *Phys. Rev. Lett.* **118**, 038001 (2017).
90. S. K. Nandi, G. Biroli, J.-P. Bouchaud, K. Miyazaki, D. R. Reichman, Critical dynamical heterogeneities close to continuous second-order glass transitions. *Phys. Rev. Lett.* **113**, 245701 (2014).
91. C. Rainone, P. Urbani, H. Yoshino, F. Zamponi, Following the evolution of hard sphere glasses in infinite dimensions under external perturbations: Compression and shear strain. *Phys. Rev. Lett.* **114**, 015701 (2015).
92. A. Wisitsorasak, P. G. Wolynes, On the strength of glasses. *Proc. Natl. Acad. Sci. U.S.A.* **109**, 16068–16072 (2012).
93. P. K. Jaiswal, I. Procaccia, C. Rainone, M. Singh, Mechanical yield in amorphous solids: A first-order phase transition. *Phys. Rev. Lett.* **116**, 085501 (2016).
94. I. Procaccia, C. Rainone, M. Singh, Mechanical failure in amorphous solids: Scale-free spinodal criticality. *Phys. Rev. E* **96**, 032907 (2017).
95. R. L. Moorcroft, S. M. Fielding, Shear banding in time-dependent flows of polymers and wormlike micelles. *J. Rheol.* **58**, 103–147 (2014).
96. S. M. Fielding, Triggers and signatures of shear banding in steady and time-dependent flows. *J. Rheol.* **60**, 821–834 (2016).
97. W. Prager, *Introduction to Mechanics of Continua* (Ginn & Co., Boston, MA, 1961).
98. K. von Hohenemser, W. Prager, Über die ansätze der mechanik isotroper kontinua. *J. Appl. Math. Mech./Z. Angew. Math. Mech.* **12**, 216–226 (1932).
99. J. G. Oldroyd, *A Rational Formulation of the Equations of Plastic Flow for a Bingham Solid* (Cambridge University Press, 1947), vol. 43, pp. 100–105.
100. M. Dinkgreve, M. M. Denn, D. Bonn, "Everything flows?": Elastic effects on startup flows of yield-stress fluids *Rheol. Acta* **56**, 189–194 (2017).
101. K. Kamani, G. J. Donley, S. A. Rogers, Unification of the rheological physics of yield stress fluids. *Phys. Rev. Lett.* **126**, 218002 (2021).
102. P. Sollich, F. Lequeux, P. Hébraud, M. E. Cates, Rheology of soft glassy materials. *Phys. Rev. Lett.* **78**, 2020 (1997).
103. S. M. Fielding, P. Sollich, M. E. Cates, Aging and rheology in soft materials. *J. Rheol.* **44**, 323–369 (2000).
104. P. Sollich, Rheological constitutive equation for a model of soft glassy materials. *Phys. Rev. E* **58**, 738 (1998).
105. J. Goyon, G. Annie Colin, A. A. Ovarlez, L. Bocquet, Spatial cooperativity in soft glassy flows. *Nature* **454**, 84–87 (2008).
106. L. Bocquet, A. Colin, A. Ajdari, Kinetic theory of plastic flow in soft glassy materials. *Phys. Rev. Lett.* **103**, 036001 (2009).
107. R. Benzi *et al*., Unified theoretical and experimental view on transient shear banding. *Phys. Rev. Lett.* **123**, 248001 (2019).
108. K. van der Vaart *et al*., Rheology of concentrated soft and hard-sphere suspensions. *J. Rheol.* **57**, 1195–1209 (2013).
109. M. Mahmoudabadbozchelou, K. M. Kamani, S. A. Rogers, S. Jamali, Unbiased construction of constitutive relations for soft materials from experiments via rheology-informed neural networks. *Proc. Natl. Acad. Sci. U.S.A.* **121**, e2313658121 (2024).
110. N. W. Tschoegl, *The Phenomenological Theory of Linear Viscoelastic Behavior* (Springer, Berlin/Heidelberg, Germany, 1989).
111. K. M. Kamani *et al*., Understanding the transient large amplitude oscillatory shear behavior of yield stress fluids. *J. Rheol.* **67**, 331–352 (2023).
112. S. A. Rogers, B. M. Erwin, D. Vlassopoulos, M. Cloitre, A sequence of physical processes determined and quantified in LAOS: Application to a yield stress fluid. *J. Rheol.* **55**, 435–458 (2011).
113. G. J. Donley, W. W. Hyde, S. A. Rogers, F. Nettesheim, Yielding and recovery of conductive pastes for screen printing. *Rheol. Acta* **58**, 361–382 (2019).
114. G. J. Donley, J. R. de Bruyn, G. H. McKinley, S. A. Rogers, Time-resolved dynamics of the yielding transition in soft materials. *J. Nonnewton. Fluid Mech.* **264**, 117–134 (2019).
115. A. N. M. Le, M. Y. Erturk, Y. H. Shim, S. A. Rogers, J. Kokini, A critical study of the nonlinear rheological properties in major classes of foods using the sequence of physical processes (SPP) method and the Fourier transform coupled with Chebyshev decomposition (FTC) method. *Food Res. Int.* **174**, 113587 (2023).

116. M. Y. Erturk, S. A. Rogers, J. Kokini, Comparison of sequence of physical processes (SPP) and Fourier transform coupled with Chebyshev polynomials (FTC) methods to interpret large amplitude oscillatory shear (LAOS) response of viscoelastic doughs and viscous pectin solution. *Food Hydrocolloids* **128**, 107558 (2022).
117. J. Kim, D. Merger, M. Wilhelm, M. E. Helgeson, Microstructure and nonlinear signatures of yielding in a heterogeneous colloidal gel under large amplitude oscillatory shear. *J. Rheol.* **58**, 1359–1390 (2014).
118. R. Radhakrishnan, S. M. Fielding, Shear banding in large amplitude oscillatory shear (LAOStrain and LAOStress) of soft glassy materials. *J. Rheol.* **62**, 559–576 (2018).
119. S.-Q. Wang et al., New experiments for improved theoretical description of nonlinear rheology of entangled polymers. *Macromolecules* **46**, 3147–3159 (2013).
120. S. Ravindranath, S.-Q. Wang, What are the origins of stress relaxation behaviors in step shear of entangled polymer solutions? *Macromolecules* **40**, 8031–8039 (2007).
121. C.-W. Lee, S. A. Rogers, A sequence of physical processes quantified in LAOS by continuous local measures. *Kor.-Austr. Rheol. J.* **29**, 269–279 (2017).
122. J. Choi, S. A. Rogers, Optimal conditions for pre-shearing thixotropic or aging soft materials. *Rheol. Acta* **59**, 921–934 (2020).
123. B. Flavio Di Dio, F. Khabaz, R. T. Bonnecaze, M. Cloitre, Transient dynamics of soft particle glasses in startup shear flow. Part II: Memory and aging. *J. Rheol.* **66**, 717–730 (2022).
124. R. Benzi *et al*., Stress overshoots in simple yield stress fluids. *Phys. Rev. Lett.* **127**, 148003 (2021).
125. R. R. Fernandes, D. E. V. Andrade, A. T. Franco, C. O. R. Negrão, Influence of pre-shearing on rheometric measurements of an oil-based drilling fluid. *Rheol. Acta* **56**, 743–752 (2017).
126. K. Kamani, S. Rogers, "Dataset for Brittle and ductile yielding in soft materials." Mendeley Data, V1. http://doi.org/10.17632/2sdvr9v4j6.1. Accessed 9 May 2024.